AIAA 81-4158

Three-Dimensional Oscillatory Piecewise Continuous-Kernel Function Method—Part III: Wings with Geometrical Discontinuities

I. Lottati* and E. Nissim†
Technion—Israel Institute of Technology, Haifa, Israel

The piecewise continuous-kernel function method is applied to wings with geometrical discontinuities. These discontinuities include leading-edge extension, leading-edge and trailing-edge control surface rotations, and gaps of various sizes around the trailing-edge control surface. In all cases, the results obtained are compared with those obtained by the vortex- or doublet-lattice methods. These results indicate the effectiveness of the present method and the inability of the lattice methods to produce results with reasonable accuracy for leading- or trailing-edge control surfaces when gaps exist about them.

Nomenclature

$\mathcal{R}$	= aspect ratio
$\Delta p(x,y)$	= pressure difference ($p_{\text{lower}} - p_{\text{upper}}$)
$\bar{\Delta p}(\bar{x},\bar{y})$	= pressure difference for the reverse flow problem
s	= area of the wing
$\bar{s}$	= area of the leading edge control surface
$w(x,y)$	= downwash (boundary condition)
$\bar{w}(\bar{x},\bar{y})$	= downwash for the reverse flow problem
(x,y)	= Cartesian coordinate
$(\bar{x},\bar{y})$	= Cartesian coordinate for the reverse flow problem
(ζ,η)	= Cartesian coordinate system corresponding to (x,y)
Λ	= wing's sweep angle (of midchord)
λ	= taper ratio

Introduction

THE piecewise continuous-kernel function[1,2] method (PCKFM) has been proposed in an attempt to extend the rapid convergence and high-accuracy characteristics of the kernel function method to wings with geometrical discontinuities. As examples one can cite the discontinuities arising due to break points along the span of the wing, leading-edge (LE) extensions, and control surface rotations. The basic ideas of the PCKFM were proposed in Refs. 1 and 2 and shown to yield excellent results for the two-dimensional case. The initial problems associated with the extension of the method to three-dimensional flows had been treated in Refs. 3 and 4 and the many numerical examples computed were limited to wings with no geometrical discontinuities (discontinuities permitted only at the wing root). In this paper the problems associated with the geometrical discontinuities of the wing will be treated and numerical examples will be included to illustrate the special characteristics of the proposed method. These problems include the determination of the piecewise continuous regions (often referred to as "boxes") and the determination of the collocation points associated with the different orthogonal polynomials employed in the various boxes. The numerical techniques developed in Ref. 3 were found to be adequate and no modifications were needed for the present work. The methodology of the present work follows lines identical to those used in Refs. 1-4.

Received Jan. 7, 1980; revision received July 22, 1980.

*Lecturer, Department of Aeronautical Engineering.

†Professor, Department of Aeronautical Engineering. Member AIAA.

Pressure Polynomials and Their Associated Collocation Points

As already stated in the earlier stages of development of the PCKFM,[1-4] the pressure singularities are assumed to be known only along the boundaries of the wing. All other pressure singularities (which coincide with the locations of the geometrical discontinuities) need not be known and are not considered in the analysis. However, in order to preserve the pressure continuity within each box, all geometrical discontinuities must lie only along the boundaries of the different boxes and must never be located within any of the boxes. Figure 1 which relates to a wing with partial span LE and TE control surfaces (with no gaps) can be used to illustrate the different orthogonal polynomials employed by the PCKFM. Figure 1 also represents the smallest number of boxes that need to be used by the present method. In the chordwise direction, boxes I and V will employ pressure polynomials orthogonal to both the LE and TE singularities, box II will employ pressure polynomials orthogonal to the LE singularity, box IV will employ pressure polynomials orthogonal to the TE singularity, and box III will employ Legendre polynomials which are orthogonal to a unit weight function. In case of gaps between the control surfaces and the wing (see Fig. 2), boxes I-V will all employ chordwise pressure polynomials orthogonal to both the LE and TE singularities. For the spanwise direction, assuming control surfaces with and without gaps (Figs. 1 and 2), boxes I-IV will use the Legendre pressure polynomials, whereas box V will use polynomials orthogonal to the wing-tip singularity (i.e., $\sqrt{1-\eta}$). In case of spanwise gaps between the control surfaces and the wing, boxes I and V will each have to be subdivided into three boxes in a fashion similar to boxes II-IV. The nine resulting boxes are illustrated in Fig. 3. Referring to Fig. 3, boxes I, III, and VIII will employ spanwise pressure polynomials orthogonal to the wing-tip singularity $\sqrt{1-\eta}$ (with $\eta=1$ at the outboard boundary of each box), boxes IV, VI, VII, and IX will employ pressure polynomials orthogonal to the tip singularity $\sqrt{1-\eta^2}$ (with $\eta=\pm 1$ at the spanwise boundaries of each box), and boxes II and V will employ the Legendre polynomials to describe the pressure distributions. In the chordwise direction boxes I, IV, and VII will employ polynomials orthogonal to the LE singularity; boxes II, V, and VIII will employ Legendre polynomials; and boxes III, VI, and IX will employ polynomials orthogonal to the TE singularity.

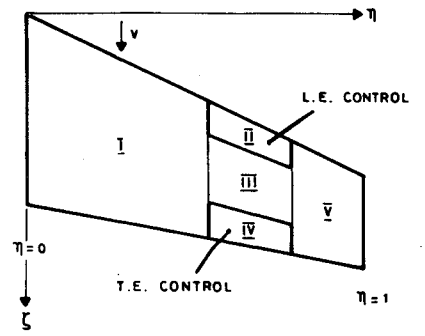

Fig. 1 Box layout for wing with partial control surfaces and no gaps.

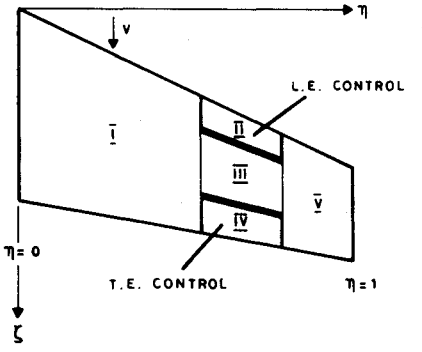

Fig. 2 Box layout for wing with partial control surfaces with a gap in chordwise direction and no gaps in spanwise direction.

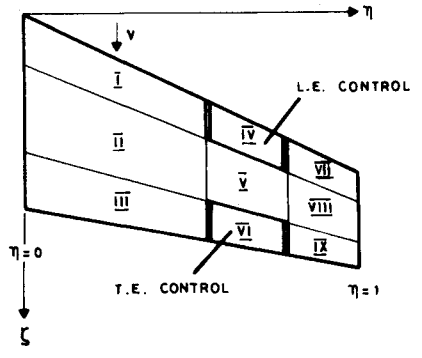

Fig. 3 Box layout for wing with partial control surfaces with a gap in spanwise direction and no gap in chordwise direction.

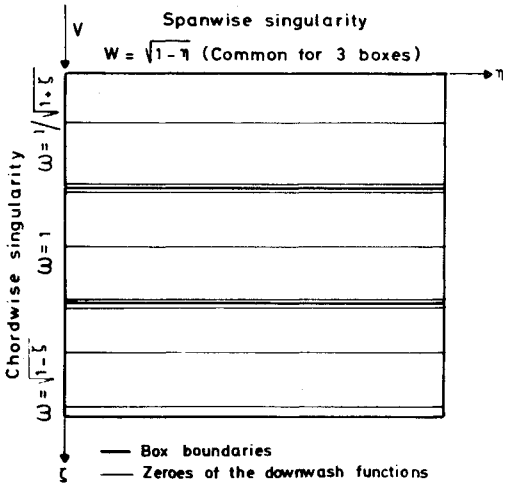

Fig. 4 Location of the zeros of downwash functions using different orthogonal pressure polynomials corresponding to wing with three chordwise boxes.

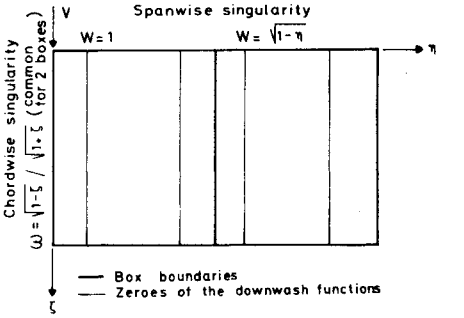

Fig. 5 Location of the zeros of downwash functions using different orthogonal pressure polynomials corresponding to wing with two spanwise boxes.

The determination of the optimum collocation points associated with the different types of pressure polynomials follows lines identical to those used in Refs. 2-5. The results obtained confirm many of the results obtained in earlier works,[1-4] the main points of which will briefly be restated here. For the chordwise direction, the collocation points are located at essentially the same points as in the two-dimensional case,[1,2] thus implying that a pressure polynomial of order m yields m collocation points for a box with LE singularity only, whereas in both the intermediate and TE boxes (with no LE singularity) the pressure polynomials of order m yield $m+1$ collocation points (see Fig. 4). These results were shown in the two-dimensional case[1,2] to require an additional collocation point for the intermediate and TE boxes, and led to the introduction of a least-squares analysis to reduce the number of the resulting equations to the number of unknown pressure coefficients. The above results for the three-dimensional case imply that procedures similar to those found for the two-dimensional case will have to be used.

For the spanwise direction, such an increase in the number of collocation points beyond the number of the unknown pressure polynomial coefficients is never found. For boxes with wing-tip singularity of the form $\sqrt{1-\eta}$ the collocation points obtained are identical to those found in Ref. 3, and for boxes using the Legendre polynomials the collocation points obtained coincide with the zeros of these same polynomials. Figure 5 shows the location of some collocation points for a two-box wing (in the spanwise direction). For boxes having singularities of the form of $\sqrt{1-\eta^2}$, the Multhopp points were taken as the collocation points.

Preliminary Results

The main objective of the preliminary results presented here is to test the validity (in the three-dimensional case) of some of the results obtained in earlier works[1,2] regarding both the box allocations and the number of collocation points.

Table 1 shows the effects on the aerodynamic coefficients of the additional chordwise collocation points mentioned in the previous section for a rectangular wing ($AR = 1$) having a 23.4% chord (full span) TE control surface. The wing is divided in this case into two boxes (wing box as the first box and TE surface as the second box).

Table 1 shows that the largest effect of the additional collocation point in the TE box is on the control surface derivatives, yielding considerable changes in values with the increase in number of the chordwise polynomials. Hence the two-dimensional results concerning the importance of these additional collocation points are reconfirmed for the three-dimensional case.

Table 2 shows the effects on the aerodynamic derivatives of increasing the number of boxes, in both the chordwise and spanwise directions, for a delta wing ($AR = 2$) with no geometrical discontinuities along its span. It can be seen that the increase in the number of boxes, beyond the minimum of one box required by the present method, leads to negligible

Table 1 Influence of an additional collocation point in the TE box on the aerodynamic coefficients for a rectangular wing with a TE flap in a steady incompressible flow[a]

No. of pressure polynomials Chordwise	Spanwise	C_{L_α}	$C^b_{M_\alpha}$	C_{L_δ}	$C^b_{M_\delta}$	CPU, s
Without an additional collocation point in the TE box						
4	4	−1.461	−0.488	−1.261	−1.411	25.58
4	3	−1.462	−0.488	−1.232	−1.445	36.12
5	3	−1.462	−0.489	−1.077	−1.257	56.35
With an additional collocation point in the TE box						
3	3	−1.461	−0.488	−1.129	−1.380	29.85
4	3	−1.462	−0.488	−1.113	−1.385	39.01
5	3	−1.462	−0.488	−1.105	−1.375	70.79

[a] The wing is divided into two boxes with identical number of pressure polynomials in each box. [b] The moment is about the wing's LE with reference chord = 1 and ℄ chord = 2.

Table 2 Influence on the aerodynamic coefficients of the number of boxes on the wing for a delta wing ($\mathcal{A}R$ = 2 in steady incompressible flow)

No. of spanwise boxes	No. of chordwise boxes	No. of pressure polynomials Chordwise	Spanwise	C_{L_α}	$C^a_{M_\alpha}$	CPU,s
Influence of chordwise division into equal sized boxes (with an additional collocation point in the intermediate and TE boxes)						
1	1	3	3	−2.204	−2.601	8.02
1	1	8	3	−2.200	−2.595	37.40
1	2	4	3	−2.208	−2.601	37.50
		4	3			
1	3	3	3			
		3	3	−2.208	−2.605	63.52
		3	3			
Influence of spanwise division into equal sized boxes						
1	1	3	3	−2.204	−2.601	8.02
1	1	3	8	−2.204	−2.605	24.95
2	1	3	4	−2.210	−2.613	26.18
		3	4			
3	1	3	3			
		3	3	−2.208	−2.602	46.12
		3	3			

[a] The moment is about the wing's apex with reference chord = 1 and ℄ chord = 2.

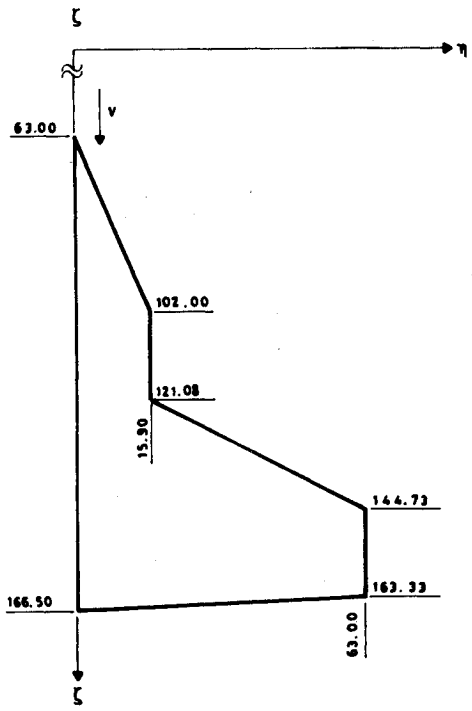

Fig. 6 Plan view of wing of YF-17 aircraft.

changes in the values of the derivatives and to a considerable increase in computational time. Here again, the conclusion reached at in the two-dimensional case[1,2] is found to hold also for the three-dimensional case, namely, that in allocating the boxes on the wing, one should aim at choosing the smallest number of boxes permissible by the present method.

Results for Wings with Geometrical Discontinuities

Discontinuities in the Chord Distribution along the Span of the Wing

As an example of this class of problems, the wing of the YF-17 aircraft will be considered.

Figure 6 shows a plan view of the wing of the YF-17 aircraft, where the discontinuity due to the LE extension can be observed. Attempts will now be made to represent the wing by different box allocations and to follow their effects on the values of the aerodynamic coefficients of the wing. Figure 7 shows four different box allocations. Figure 7a is given as an example where the minimum number of boxes required by the present method is violated. Clearly, a box boundary should be located at the geometrical discontinuity to create two boxes, as shown in Fig. 7b. In both Figs. 7a and 7b, it is possible to account for the LE, TE, and wing-tip singularities but impossible to allow for the pressure singularity (of wing-tip type) at the spanwise edge of the LE extension. The box allocation in Fig. 7c permits the introduction of the above wing-tip type of singularity along the right-hand boundary of box I in addition to the other wing boundary singularities. Figure 7c

Table 3 Influence on the aerodynamic coefficients of the boundary conditions at the spanwise edge of the LE extension for the YF-17 wing in steady incompressible flow

Fig. ref.	No. of boxes	No. of pressure polynomials Chordwise	Spanwise	C_{L_α}	$C^a_{M_\alpha}$	CPU,s	Remarks
7a	1	3	3	−2.620	−271.9	8.50	
	1	6	6	−2.363	−244.2	81.81	
7b	2	3 3	3 3	−2.955	−202.3	22.76	
	2	6 6	3 3	−3.091	−212.4	88.78	
7c							
	3	3 3 3	3 3 3	−2.948	−202.3	40.73	Without imposing the boundary condition at the spanwise edge of the LE extension
	3	3 3 3	3 3 3	−2.798	−192.3	52.75	With imposing the boundary condition at the spanwise edge of the LE extension
7d							
	3	3 3 3	3 2 3	−2.953	−202.3	32.40	
	3	3 3 3	3 3 3	−2.941	−203.1	32.40	Computed by using the reverse flow theorem
		144 vortex-lattice boxes		−3.004	−206.8	75.02	

[a] The moment is about the wing's apex with reference chord = 1 and ℄ chord = 103.5.

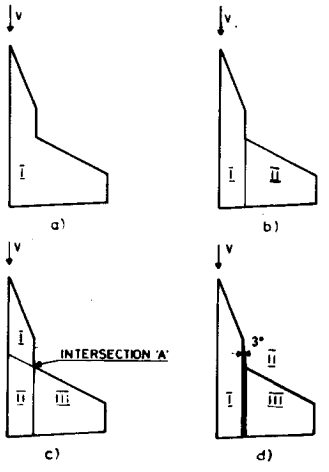

Fig. 7 Plan view of wing of YF-17 aircraft with four different box allocations.

introduces, however, a difficulty arising as a result of imposing conflicting requirements; the boundary conditions of box I require the pressure to assume zero values along the outboard tip of box I, whereas those of box III require the pressure to assume infinite values along its LE. Hence, conflicting requirements are imposed at intersection A (see Fig. 7c). It may therefore be preferable either to ignore the wing-tip requirements of the pressure in box I (Fig. 7c) or else to create a fictitious box which will transform the wing tip of box I into a LE, as shown in Fig. 7d.

Table 3 shows the results obtained by applying the present method to the different box allocations just described. It can be clearly seen that the box allocation represented by Fig. 7a gives the worst results. Somewhat better results are obtained using the box allocations represented by Figs. 7b and 7c. The best results are obtained using the box allocation represented by either Fig. 7d or Fig. 7c, but avoiding the conflicting requirements by ignoring the wing-tip type of singularity of box I (Fig. 7c).

To test the accuracy of the results, reverse flow analysis was introduced. In the reverse flow analysis, the box allocation shown by Fig. 7c presents no difficulties at intersection A, since the pressure along all adjoining boundaries is zero.

The reverse flow theorem[6] gives the following relationship between direct and reverse flow pressures

$$\int_s \int \bar{w}(\bar{x},\bar{y})\,\Delta p(x,y)\,\mathrm{d}x\mathrm{d}y = \int_s \int w(x,y)\,\overline{\Delta p}(\bar{x},\bar{y})\,\mathrm{d}\bar{x}\mathrm{d}\bar{y} \quad (1)$$

where $\bar{w}(\bar{x},\bar{y})$ represents any chosen boundary condition for the reverse flow problems and the integral is taken over the surface of the wing. Hence, by choosing

$$\bar{w}(\bar{x},\bar{y}) = w(x,y) = 1$$

the pressure integral over the wing in the reverse flow [right-hand side of Eq. (1)] yields the lift force acting over the wing in the direct flow [left-hand side of Eq. (1)]. A similar procedure can be adopted for the moment by choosing

$$w(x,y) = 1$$

$$\bar{w}(\bar{x},\bar{y}) = \bar{x}$$

and substituting into Eq. (1) to obtain the following relationship

$$\int_s \int \bar{x}\,\Delta p(x,y)\,\mathrm{d}x\mathrm{d}y = \int_s \int \overline{\Delta p}(\bar{x},\bar{y})\,\mathrm{d}\bar{x}\mathrm{d}\bar{y}$$

Hence the lift force acting on the wing in the reverse flow is equal to the moment acting on it in the direct flow. It can thus be seen that the required aerodynamic derivatives are all obtained by integrating the reverse flow pressures where no conflicting requirements exist. The agreement between the reverse and the direct flow results are excellent for the box allocation represented by Fig. 7c (with no contradictory requirements), and Fig. 7d.

For purposes of comparison, Table 3 also gives the results obtained using the vortex-lattice method[7] with 144 boxes. The agreement between the two methods is seen to be good.

Table 4 Relative convergence of the aerodynamic coefficients as computed by the PCKFM and by the vortex-lattice method for a rectangular wing ($\mathcal{R}=1$) with a TE flap (22.5% chord) in steady incompressible flow

PCKFM					
No. of pressure polynomials[a]					
Chordwise	Spanwise	C_{L_δ}	$C^b_{M_\delta}$	C_{H_δ}	CPU,s
2[c]	2	−1.144	−1.334	−0.0411	12.16
2	2				
3	3	−1.117	−1.379	−0.0438	29.82
3	3				
4	3	−1.101	−1.384	−0.0460	32.42
3	3				
5	3	−1.093	−1.384	−0.0473	39.32
3	3				
6	3	−1.088	−1.383	−0.0482	47.68
3	3				
5	5	−1.092	−1.381	−0.0467	53.65
5	5				
Vortex-lattice method					
No. of boxes[a]					
Chordwise	Spanwise	C_{L_δ}	$C^b_{M_\delta}$	C_{H_δ}	CPU,s
9[c]	8	−1.092	−1.421	−0.0601	15.32
3	8				
9	12	−1.074	−1.401	−0.0593	58.96
3	12				
9	16	−1.066	−1.391	−0.0588	116.97
3	16				

[a] The moment is about the wing's LE with reference chord = 1 and ℄ chord = 2. [b] The wing is divided into two chordwise boxes and no spanwise subdivisions. [c] 2 refers to the fore box (wing); 2 refers to the aft box (TE flap).

Table 5 Comparison of the convergence of aerodynamic coefficients computed by the PCKFM and by the vortex-lattice method for a rectangular wing ($\mathcal{R}=1$) with a LE flap (22.5% chord) in steady incompressible flow

PCKFM					
No. of pressure polynomials[a]					
Chordwise	Spanwise	C_{L_β}	$C^b_{M_\beta}$	C_{H_β}	CPU,s
Direct flow					
2[c]	2	0.0558	−0.309	0.0401	12.26
2	2				
3	3	0.0291	−0.320	0.0507	26.71
3	3				
3	3	0.0355	−0.293	0.0509	32.37
4	3				
3	3	0.0328	−0.289	0.0515	39.46
5	3				
3	3	0.0305	−0.286	0.0520	47.89
6	3				
5	3	0.0328	−0.290	0.054	54.47
5	3				
Reverse flow					
3	3	0.0307	−0.305		29.82
3	3				
3	3	0.0293	−0.271		32.42
4	3				
3	3	0.0297	−0.269		39.32
5	3				
3	3	0.0294	−0.270		53.65
6	3				
Vortex-lattice method					
No. of boxes					
Chordwise	Spanwise	C_{L_β}	$C^b_{M_\beta}$	C_{H_β}	CPU,s
3[c]	8	0.0376	−0.313	0.209	23.43
9	8				
3	12	0.0365	−0.309	0.207	59.52
9	12				
3	16	0.0360	−0.308	0.205	114.03
9	16				

[a] The moment is about the wing's LE with reference chord = 1 and ℄ chord = 2. [b] The wing is divided into two chordwise boxes and no spanwise subdivisions. [c] 2 refers to the fore box (LE flap); 2 refers to the aft box (wing).

Discontinuities Due to Control Surface Deflections

In this section, the PCKFM will be applied to wings with LE and TE control surfaces, with and without gaps.

Table 4 gives a comparison of the convergence of the aerodynamic coefficients computed by the present method and by the vortex-lattice method for a rectangular wing with a full span, 22.5% chord, TE control (with no gaps). The coefficients relating to the wing have been treated earlier in this work while testing the effects of increasing the number of boxes beyond the one required by the geometrical discontinuities. Table 4 therefore focuses on the control surface derivatives only (as will be done throughout this section). As can be seen, the convergence of the present method is rapid and its agreement is good in comparison with the results obtained using the vortex-lattice method, with the exception of the control surface hinge moment coefficient. The experience obtained while treating the two-dimensional case[1,2] indicates that the results obtained by the present method are considerably more accurate than those obtained by the vortex-lattice method, especially regarding control surface derivatives. This increase in accuracy originates from the employment of orthogonal polynomials in all boxes and from the imposition of the wing boundary singularities.

Table 5 shows the results pertaining to the same wing as in Table 4 but having a full span, 22.5% chord, LE control surface (with no gaps). The convergence of $C_{M\beta}$ and $C_{H\beta}$ appears to be rapid; however, the convergence of $C_{L\beta}$ as obtained by the present method appears to be rather slow. This slow convergence is a result of the two following counteracting effects: The downward rotation of the LE control surface leads on the one hand to a decrease in lift due to the effective decrease in the angle of attack of the whole wing whereas, on the other hand, this same control surface rotation leads to an increase in lift due to the effective increase in the wing's camber. Since these two counteracting effects are of the same order of magnitude, the resulting net lift is small and therefore sensitive to small changes caused by changing the number of pressure polynomials.

Table 5 indicates that for LE control surfaces, more polynomials should be used to describe the pressure distribution on the wing compared to the number of polynomials required to describe the pressure distribution on the LE control surface. Here again, reverse flow considerations are used to determine the converged values for the LE aerodynamic coefficients (this procedure may be adopted as a standard procedure for LE control surfaces). This is done as follows.

For direct flow, let

$$w(x,y)=\begin{cases}1 \text{ on the LE control}\\ 0 \text{ outside the LE control}\end{cases}$$

and for the reverse flow, let

$$\bar{w}(\bar{x},\bar{y})=1 \text{ throughout the wing}$$

Substitution of the above values into the reverse flow ex-

Table 6 Influence on the aerodynamic coefficients of the gap between the wing and the flap as computed by the PCKFM in a steady incompressible flow (see wing in Fig. 10)

No. of boxes	No. of pressure polynomials (for each box) Chordwise	Spanwise	C_{L_α}	$C^a_{M_\alpha}$	$C_{H_\alpha}\cdot 10^{-3}$	C_{L_δ}	$C^a_{M_\delta}$	$C_{H_\delta}\cdot 10^{-2}$	CPU,s
Partial spanwise flap (31% chord, 22% span) with no gap									
4 (min for PCKFM)	3	3	−1.089	−2.063	−0.89	−0.163	−0.530	−0.530	41.69
172 boxes on wing and 18 boxes on flap (vortex-lattice method)			−1.134	−2.178	−1.79	−0.164	−0.531	−0.510	112.62
Partial spanwise flap (30% chord, 20% span) with 1% gap (all around)									
6 (min for PCKFM)	3	3	−1.083	−2.034	−0.57	−0.072	−0.235	−0.190	87.36
172 boxes on wing and 18 boxes on flap (vortex-lattice method)			−1.134	−2.168	−1.29	−0.118	−0.387	−0.330	117.25
Partial spanwise flap (26% chord, 12% span) with 5% gap (all around)									
6 (min for PCKFM)	3	3	−1.105	−2.067	−0.12	−0.021	−0.070	−0.370	87.02
180 boxes on wing and 10 boxes on flap (vortex-lattice method)			−1.145	−2.165	−0.24	−0.035	−0.117	−0.740	118.05

[a] The moment is about the wing's apex with reference chord = 1 and ℄ chord = 4. Reference area does not include the area of the gap.

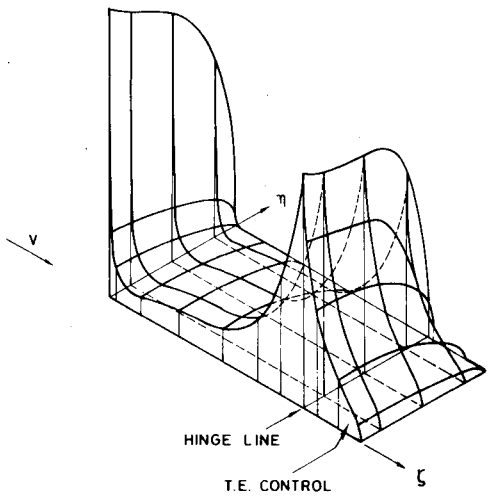

Fig. 8 Pressure distribution due to TE control surface rotation (for steady incompressible flow).

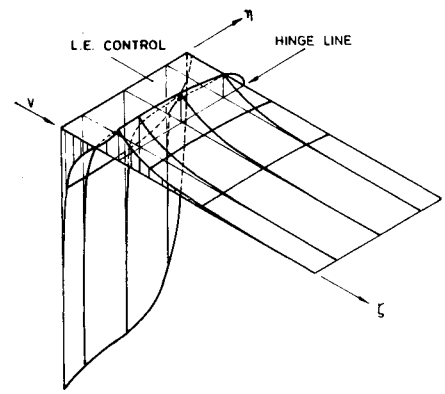

Fig. 9 Pressure distribution due to LE control surface rotation (for steady incompressible flow).

pression given by Eq. (1) yields

$$\int_s \int \Delta p(x,y)\,dx dy = \int_{\bar{s}} \int \overline{\Delta p}(\bar{x},\bar{y})\,d\bar{x}d\bar{y} \qquad (2)$$

where $\bar{s}$ represents the area of the LE control surface only. Hence, the lift due to the rotation of the LE control surface is obtained by integrating over the control surface only, the reverse flow pressure due to a unit downwash throughout the wing (i.e., no control surface discontinuities). Similar techniques can be applied for the moment and, as already stated, its convergence is very rapid. It is interesting to note that the results obtained in this case by the vortex-lattice method show a large deviation from the results obtained by the present method. These latter results have been verified through the use of the reverse flow analysis and are considered to represent the correct values. The pressure distribution due to the TE control surface rotation is shown in Fig. 8, and the pressure distribution due to the rotation of the LE control surface is shown in Fig. 9. These pressure distributions confirm some of the statements made above.

Table 6 shows the influence of the gap between the wing and the partial span TE control surface on the aerodynamic coefficients computed by the present method and those computed by the vortex-lattice method. The wing used is a swept back wing with $\Lambda = 56.3$ deg, $AR = 0.727$, and a taper ratio $\lambda = 0.375$ (see Fig. 10). The first part of Table 6 gives the aerodynamic coefficients for a wing with a control surface and no gaps. The agreement between the results obtained by the present method and those obtained by the vortex-lattice method are excellent (except for C_{H_α} which is very small in value). A 1% wing chord gap is now permitted on all sides of the TE control surface (thus reducing its chord size to 30% of the wing chord). Table 6 shows that the gap has a negligible effect on the values of $C_{L\alpha}$ and $C_{M\alpha}$ computed by the two methods mentioned earlier. However, the effect of the 1% gap on the TE control surface derivative is very large when compared to those with the zero gap. Furthermore, the difference in this case between the results obtained by the present method and those obtained by the vortex-lattice method for the TE control derivatives is very large. Similar behavior can be seen when the gap is further increased to 5% of the chord (thus reducing the chord of the TE control to 26% of the wing chord). Note that while increasing the gaps, the wing area is reduced, thus causing some increase in the values of the aerodynamic derivatives. An inspection of Fig. 11, which shows the pressure distributions over the wing due to the TE control rotation (with 1% gap) using the above-mentioned methods, shows that the vortex-lattice method yields higher results due to the violation of the boundary conditions on both the wing itself (especially near the control surface hinge line) and the control surface (especially near its tips). This result is of major importance since gaps do exist on all control surfaces and since their consideration by the vortex-lattice method seems to yield results having insufficient accuracy.[8]

For the sake of completeness, the PCKFM is applied to an oscillating rectangular wing (with $AR = 1$ and $k = 1$), having a

Table 7 Relative convergence of the aerodynamic coefficients as computed by the PCKFM and by the doublet-lattice method for a rectangular wing ($\mathcal{R}=1$) with a TE flap (22.5% chord) in unsteady[d] incompressible flow ($k=1, M=0$)

PCKFM						Doublet-lattice method					
No. of pressure polynomials[a] Chordwise	Spanwise	C_{L_δ} (deg)	$C^c_{M_\delta}$ (deg)	C_{H_δ} (deg)	CPU,s	No. of boxes Chordwise	Spanwise	C_{L_δ} (deg)	$C^c_{M_\delta}$ (deg)	C_{H_δ} (deg)	CPU,s
2[b]	2	1.305 (219.0)	1.647 (225.6)	0.0827 (248.7)	13.14	5[b]	8	1.130 (212.1)	1.562 (215.2)	0.0905 (233.1)	54.45
2	2					3	8				
3	3	1.232 (215.4)	1.624 (220.2)	0.0839 (246.4)	30.80	9	8	1.152 (212.2)	1.585 (212.2)	0.0884 (235.0)	124.17
3	3					3	8				
4	3	1.203 (214.1)	1.612 (218.6)	0.0845 (244.8)	35.87	9	12	1.135 (212.2)	1.562 (215.7)	0.0873 (235.1)	279.24
3	3					3	12				
5	3	1.191 (213.8)	1.602 (218.1)	0.0848 (243.9)	41.96	9	16	1.126 (212.2)	1.550 (215.7)	0.0867 (235.1)	525.98
3	3					3	16				
6	3	1.185 (213.6)	1.600 (217.8)	0.0850 (243.5)	50.94						
3	3										
5	5	1.191 (213.8)	1.600 (218.1)	0.0837 (244.6)	97.17						
5	5										

[a] The wing is divided into two chordwise boxes and no spanwise subdivisions. [b] 2 refers to the fore box (wing); 2 refers to the aft box (TE flap). [c] The moment is about the wing's LE with reference chord = 1 and ℄ chord = 2. [d] The control surface oscillates about LE with reduced frequency $k=\omega/v$.

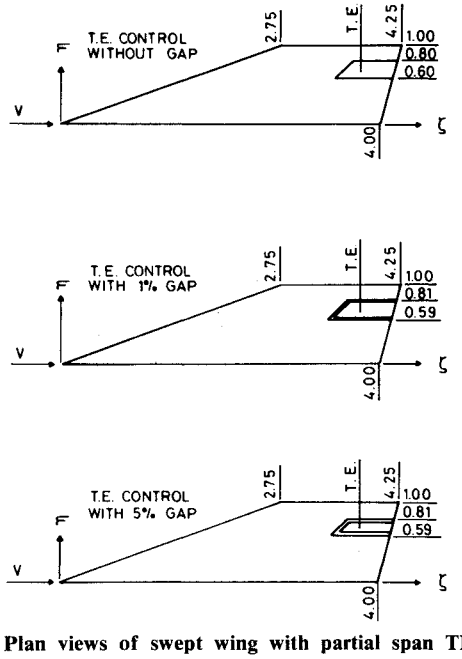

Fig. 10 Plan views of swept wing with partial span TE control surface with and without gaps.

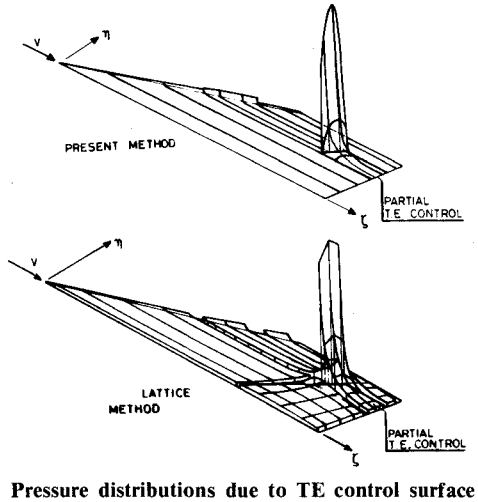

Fig. 11 Pressure distributions due to TE control surface rotation (with 1% gap all around) obtained using the vortex-lattice and the present methods.

23.5% chord, full span, TE control surface in incompressible flow. Table 7 shows the convergence of the aerodynamic coefficients computed by the present method as a function of the number of pressure polynomials assumed in each box. As can be seen from the comparison of the results computed by the present method and those computed using the doublet-lattice method (based on the vortex-lattice method for $k=0$), the computational time involved using the present method is considerably shorter than that required by the doublet-lattice method.

Conclusion

Few examples relating to wings with geometrical discontinuities were computed using the PCKFM and the results obtained were compared with those obtained using the lattice methods. The high accuracy of the PCKFM and its rapid convergence characteristics were once again demonstrated together with its inherent efficiency and reduced computational time. In most of the cases considered, the differences between the values of the aerodynamic coefficients as obtained by the different methods, including the lattice methods, and those obtained by the present method were small. In the present work, the PCKFM is shown to yield results that are considerably more accurate than those obtained using the lattice methods. These latter results relate to the important cases of LE and controls surface derivatives (with gaps around the controls). It is interesting to note that in these cases the results produced by the lattice methods are considerably larger than those produced by the PCKFM. This variation in values is attributed to the inability of the lattice methods to impose the pressure singularities along the different boundaries of the wing. This finding is of prime importance for problems associated with the performance of control surfaces, such as control surface effectiveness problems or flutter suppression problems which employ active control systems.

The examples treated herein relate to planar wings or multiwing planar configurations. The PCKFM is capable of treating nonplanar problems with no added difficulties. For the sake of brevity, the results of such applications have not been included in this paper.

Acknowledgment

This work represents part of the first author's doctoral thesis.

References

[1] Nissim, E. and Lottati, I., "Oscillatory Subsonic Piecewise Continuous Kernel Function Method," National Technical Information Service, Springfield, Va., Paper N77-73109, 1977.

[2] Nissim, E. and Lottati, I., "Oscillatory Subsonic Piecewise Continuous Kernel Function Method," *Journal of Aircraft*, Vol. 14, June 1977, pp. 515-516.

[3] Lottati, I. and Nissim, E., "Three Dimensional Oscillatory Piecewise Continuous Kernel Function Method—Part I: Basic Problems," *Journal of Aircraft*, Vol. 18, May 1981, p. 346.

[4] Lottati, I. and Nissim, E., "Three Dimensional Oscillatory Piecewise Continuous Kernel Function Method—Part II: Geometrically Continuous Wings," *Journal of Aircraft*, Vol. 18, May 1981, p. 352.

[5] Hsu, P.T., "Some Recent Developments in the Flutter Analysis of Low-Aspect-Ratio Wings," *Proceedings of National Specialist Meeting on Dynamics and Aeroelasticity*, Institute of Aeronautical Sciences, Nov. 1958, pp. 7-26.

[6] Flax, A.H., "Generalized Reverse Flow and Variational Theorems in Lifting-Surface Theory," *Journal of Aeronautical Sciences*, Vol. 19, No. 6, 1952, p. 361.

[7] Hedman, S.G., "Vortex Lattice Method for Calculation of Quasi-Steady State Loadings on Thin Elastic Wings in Subsonic Flow," Aeronautical Research Institute of Sweden, Rept. 105, Oct. 1965.

[8] Rowe, W.S., Winther, B.A., and Redman, M.C., "Prediction of Unsteady Aerodynamic Loadings Caused by Leading Edge and Trailing Edge Control Surface Motions in Subsonic Compressible Flow—Analysis and Results," NASA CR-2543, Aug. 1975.